PROCEEDINGS, Twenty-First Workshop on Geothermal Reservoir Engineering
Stanford University, Stanford, California, January 22-24, 1996
SGP-TR-151

Analysis of the Pressure Response of High Angle Multiple (HAM) Fractures Intersecting a Wellbore

Satoshi Ujo [1], Kazumi Osato [1], Ron C. Schroeder [2], and Norio Arihara [3]

1. Geothermal Energy Research and Development Co., Ltd., Tokyo, Japan
2. Berkeley Group Incorporated, CA, U.S.A.
3. Waseda University, Tokyo, Japan

ABSTRACT

Several methods have been presented in the literature for analyzing transient pressure data of fractured wells. We tested with some model studies based on the solutions to the 3D problem of multiple high-angle fractures (HAM) intersecting a wellbore. The model solutions representing transient pressure behavior of HAM fractures are defined in terms of 3D rectilinear coordinates. The HAM fracture model equations include the finite conductivity of the fractures, and our solutions reduce to previously published results for the special case of vertical fractures and/or infinite-conductivity fractures. A computer program, MULFRAC, has been provided to calculate the dimensionless drawdown at the wellbore. This paper shows the solutions of MULFRAC, some comparison of MULFRAC results with published special cases.

INTRODUCTION

This paper is a model for analysis of the pressure response of High Angle Multiple (HAM) fractures intersecting a wellbore. The geometry of the HAM fracture problem is shown in Figure 1.

Previous work on transient pressure response of fractured well has been concentrated on three model approximations. The model include vertical (Gringarten et al., 1974), horizontal (Gringarten and Ramey, 1974), and distributed fractures (Warren and Root, 1963). In all cases to date some common assumptions have been made for almost all transient well test solutions. For example the assumptions include: a)the reservoir is infinite with closed top bottom, b)the reservoir consists of homogeneous rock and fluid, c)is isotropic, d)gravity is negligible, and e)the reservoir fluid is only slightly compressible. Variations on these assumptions have been made for gas reservoir applications, and many forms of bounded reservoirs have been investigated.

Multiple fractures have been investigated also (Strubhar et al., 1975), but the fractures treated in that report in highly inclined wells, and are not similar to fractures found in geothermal reservoirs. In the latter case, the fractures (faults) are often at high angles from horizontal and the wells are only slightly or moderately inclined, resulting in penetration of multiple high angle fractures as shown in Figure 1. This study will review the existing fracture models in order to make familiar the most applicable solution processes. Then important points will be covered for the extension of the existing theories to case of High Angle Multiple (HAM) fractures penetrating the wellbore.

However, this time we didn't calculate multiple fracture with the computer program MULFRAC (current version), although the model was considered with the concept of multiple fracture. At first, we compared the MULFRAC results with published special cases about single fracture, and we investigated the property of this model based on some comparisons (vertical fracture and inclined one).

BACKGROUND OF FRACTURE MODEL

Vertical Fractures

The first solution for the finite conductivity vertical was developed by Cinco-Ley and Sameniego using the methods developed by Gringarten et al. Their solutions were obtained numerically using a discretized representations of the fracture. In 1978 Cinco and Sameniego applied the Laplace transform to the problem of the Laplace transform of the dimensionless pressure drop in terms of the Laplace variable, s, for the linear and bilinear portions of the curve are

$$L[P_{wd}]=\frac{\pi}{F_D S\sqrt{\frac{S}{\eta_D}+\frac{2\sqrt{S}}{F_D}}} \qquad (1)$$

The equation can be solved using the numerical

inverse Laplace transform. The early-time and late-time solutions can be obtained analytically and are given by

a) fracture linear flow

$$Pwd=\frac{2}{F_D}\sqrt{\pi\,\eta_D t_{Dxf}} \tag{2}$$

b) bilinear flow period

$$Pwd=\frac{\pi}{\Gamma(1.25)\sqrt{2F_D}}t_{Dxf}^{1/4} \tag{3}$$

c) formation linear flow period

$$Pwd=\sqrt{\pi\,t_{Dxf}}+\frac{\pi}{3F_D} \tag{4}$$

Horizontal Fractures

The first solution for a horizontal fracture was developed by Gringarten and Ramey using the point Green's function approach coupled with Newman's product-solution technique as they did for the vertical fracture case. The dimensionless pressure is given by

$$Pfd=\int_0^{t_{Df}}\frac{1}{HD}\frac{e^{-\frac{1}{\tau}\left(\frac{r}{H}\right)^2}}{\tau}\int_0^1 I_0\left(\frac{r\,\nu}{2r_f\tau}\right)e^{-\frac{\nu 2}{4\tau}}\,\nu\,d\nu$$
$$\left(1+2\sum_{n=1}^{\infty}e^{-\frac{n^2\pi^2\tau}{H_D^2}}\cos\left(n\pi\frac{Zf}{H}\right)\cos\left(n\pi\frac{Z}{H}\right)\right)d\tau \tag{5}$$

They calculated the effect of a rectangular fracture instead of the circular fracture of Gringarten et al. His equation is

$$Pwd=\int_0^{t_{Df}}erf\left(\sqrt{\frac{\pi F}{4\tau}}\right)$$
$$erf\left(\sqrt{\frac{\pi}{4F\tau}}\right)\frac{h_D}{2\sqrt{\tau}}\left(1+2\sum_{i=1}^{\infty}e^{-\frac{\pi i2hD2}{4\tau}}\right)d\tau \tag{6}$$

Inclined Fractures

The only analyses of inclined fractures have been by Cinco and Daneshy. Cinco used the Green's function method of Gringarten and Ramey to derive an expression for the pressure in an inclined fracture. The pressure response was calculated numerically from

$$PfD=\frac{\sqrt{\pi}}{4hwd}\int_0^{t_D}\frac{1}{\sqrt{\tau}}\left(erf\left(\frac{1+y_D}{2\sqrt{\tau}}\right)+erf\left(\frac{1-y_D}{2\sqrt{\tau}}\right)\right)I_{zD}\,d\tau \tag{7}$$

where

$$I_{zD}=\int_{-1/2hwd}^{+1/2hwd}e^{\left(-\frac{x_D^2+Z\sin\theta}{4\tau}\right)}$$
$$\left(1+2\sum_{n=1}^{\infty}e^{\left(-\frac{n2\pi2\tau}{hD2}\right)}\cos\left(\frac{n\pi Z_D}{h_D}\right)\cos\left(n\pi\left(\frac{Z\cos\theta-ZwD}{hD}\right)\right)\right)dZ \tag{8}$$

No analyses of multiple,inclined fractures has been found in the literature.

PHYSICAL MODEL OF MULTIFRACTURES MODEL

When the fracture is inclined relative to the vertical wellbore, the representation must be 3-dimensional as shown in Figure 2. For inclined fractures the intersection of the wellbore and the planar fracture is an ellipse. The elliptical intersection has the limiting cases of a circle for horizontal fractures and a full-fracture-height line for a vertical fracture. The elliptical shape of the wellbore-fracture intersection is most important for small fractures and is negligible for large fractures, i.e. when xf >> rw. In the latter case the wellbore-fracture intersection can be approximated by a line source in the plane of the fracture with length equal to the major axis of the ellipse. The wellbore intersection and fracture plane are shown in elliptic coordinates in Figure 3.

The view shown in Figure 3 is looking perpendicular to the fracture. In Figure 4 we see three views of the fracture. In the coordinate system of Figures 2 and 4 the y and z coordinates in the plane of the fracture are related by

$$z_{FP}=y_{FP}\cot(\Theta) \tag{9}$$

where FP refers to y,z values in the fracture

plane.

EQUATION OF MULTIFRACTURES MODEL

Review of the Differential Equations

The following equations satisfy the model described in this report. The symbols are defined in the previous section and in the Nomenclature, below. The pressure drawdown variables P_D and P_{Df} are the Laplace transforms, and are not the time-dependent solution. The latter is obtained numerically.

$$\frac{\partial^2 P_D}{\partial x_D^2} + \frac{\partial^2 P_D}{\partial y_D^2} + \frac{\partial^2 P_D}{\partial z_D^2} = sP_D \qquad (10)$$

In the fracture the flow is pseudo-linear. In the x direction we have

$$\frac{\partial^2 P_{Dfx}}{\partial x_D^2} + \frac{1}{F_D}\left(\frac{\partial P_D}{\partial y_D} + \frac{\partial P_D}{\partial z_D}\right)_{FP} = \frac{s}{\eta_D} P_{Dfx} \qquad (11)$$

and the y,z flow component is given by

$$\frac{\partial^2 P_{Dfy,z}}{\partial y_D^2} + \frac{\partial^2 P_{Dfy,z}}{\partial z_D^2} + \frac{1}{F_D}\left(\frac{\partial P_D}{\partial y_D} + \frac{\partial P_D}{\partial z_D}\right)_{FP} = \frac{s}{\eta_D} P_{Dfy,z} \qquad (12)$$

The inner (wellbore) boundary condition is governed by the pseudo-linear flow pattern, i.e. in the x direction for the fracture

$$F_D\left(\frac{\partial P_{Df}}{\partial x_D}\right)_{WB} = -\frac{\pi}{s} \qquad -z_{Dw} \le z_D \le +z_{Dw} \qquad (13)$$

Similarly, the formation late time has the x equation

$$\left(\frac{\partial P_D}{\partial x_D}\right)_{WB} = -\frac{\pi}{s} \qquad -z_{Dw} \le z_D \le +z_{Dw} \qquad (14)$$

Equation (13) corresponds to the one-dimensional bi-linear flow approximation used previously by Cinco et. al and for a vertical fracture, and as we show below, equation (14) corresponds to the formation-dominated flow. The symbol WB on the left hand side of equation (12) indicates that the terms must be evaluated at the "WellBore".

The initial conditions are given by

$$P_D = P_{Df} = 0 \qquad at \qquad t_{Dxf} \le 0 \qquad (15)$$

The Boundary Conditions

Since the fracture is approximated by a plane, the following condition holds

$$P_{Df} = (P_D)_{FP} \qquad (16)$$

The outer boundary conditions are

$$\left.\begin{aligned} \lim_{xD \to \infty} P_D &= 0 \\ \lim_{yD \to \infty} P_D &= 0 \end{aligned}\right\} \qquad (17)$$

and the closed reservoir condition is given by

$$\left(\frac{\partial P_D}{\partial z_D}\right)_{\pm H_D} = 0 \qquad (18)$$

where the Neumann boundary condition in equation (18) is evaluated at the top and bottom of the reservoir. The parameter, h, is the reservoir height as shown in Figure 4. In this coordinate system the rectangular parallelepiped that just encloses the fracture plane, FP, is defined by

$$\left.\begin{aligned} -x_{Df} \le x_D \le +x_{Df} \\ -y_{Df} \le y_D \le +y_{Df} \\ -z_{Df} \le z_D \le +z_{Df} \end{aligned}\right\} \qquad (19)$$

The rectangle representing the wellbore intersection with the fracture is defined by

$$\left.\begin{aligned} -r_D \le x_D \le +r_D \\ -r_D \le y_D \le +r_D \end{aligned}\right\} \qquad (20)$$

where the height of the wellbore rectangle is given by

$$z_{Dw} = r_D \cot(\theta) \qquad z_{Dw} \le 1 \qquad (21)$$

Solutions in Each Region

In the reservoir the pressure drawdown is modeled by Equation (10) for each separate region. The solutions in region I are given in terms of the region IV values (see Figure 3). For the outer portion of region I, i.e. $x_D \ge x_{Df}$, $y_D \ge y_{Df}$

$$P_{DI}^{outer} = P_{DI}^{inner}\, e^{-a(xD-xDf)}\, e^{-a(yD-yDf)} \qquad (22)$$

where P_{DI}^{inner} is evaluated on the surface defined by x_{Df} and y_{Df} between-H and 0. We see that $y_{Df} \to 0$ when the fracture angle goes to zero. As $y_{Df} \to 0$ the inner region I, and the entire region IV, are reduced to zero also. In that case the outer portion of region I gives the complete region I solution, and P_{DI}^{inner} is then the wellbore. In the latter case the z dependence is given by equation (27), below.

The region II solution is given in terms of the region IV solutions, where the boundary matching

requires that the region II solution matches at both $z_D = 0$ and $z_D = z_{Df}$ .thus we have

$$P_{DII} = (f_{Db} + f_{Da})\, e^{-a(x_D - x_{Df})}\, e^{-a(y_D - y_{Df})} \tag{23}$$

where the f functions are given by

$$f_{Db} = P_{DIV\ y\ D f z D f} \frac{\sinh(a\ z_D)}{\sinh(a\ z_{Df})} \tag{24a}$$

$$f_{Da} = P_{DIV\ y\ Df=0} \frac{\sinh(a(z_D - z_{Df}))}{\sinh(a\ z_{Df})} \tag{24b}$$

and where f_{Da} and f_{Db} are evaluated along the x and y boundaries of region IV between $z_D = 0$ and $z_D = z_{Df}$. As the fracture angle goes to zero the region multiplier in equation (23) reduces to the wellbore value.

The region III solution is given in terms of the region V surface defined by

$$x_D = x_{Df} \text{ and } y_D = y_{Df} \tag{25}$$

$$P_{DIII} = P_{DV}\, e^{-a(x_D - x_{Df})}\, e^{-a(y_D - y_{Df})}$$

The region V solution is given in terms of the region IV solution, but has a more complicated z dependence due to the closed boundary at $z_D = H_D$

$$P_{DV} = P_{DIVz} \frac{\cosh(a(H_D - z_D))}{\cosh(a(H_D - z_{Df}))} \tag{26}$$

For the inner portion of region I, i.e. $0 < x_D < x_{Df}$, $0 < y_D < y_{Df}$ we have

$$P_{DI}^{inner} = P_{DIVx,y} \frac{e^{-(a(z_D + H_D))}}{e^{-(aH_D)}} \tag{27}$$

where P_{DIV} is evaluated on the $z_D = 0$ surface of region IV. In equations (22) through (27) the value of α is given by

$$3a^2 = a^2 + b^2 \tag{28}$$

and the values of a and b are given by

$$a = \sqrt{\frac{s}{1+\tan^2(\theta)}} \tag{29a}$$

$$b = \sqrt{\frac{s}{1+\cot^2(\theta)}} \tag{29b}$$

In Region IV above and below the fracture (see Figure 4) the y,z flow is perpendicular at the fracture. Region IV is described by the partial differential equation

$$\frac{\partial^2 P_{DIV}}{\partial y_D^2} + \frac{\partial^2 P_{DIV}}{\partial z_D^2} = s\, P_{DIV} \tag{30}$$

The first y,z solution for equation] (30) is defined in region IV below the fracture plane and has a y-dependence given by

$$P_{DIV\ y} = P_{Df} \frac{e^{-(a(y_D - y_{Df}))}}{e^{-(a(y_{FP} - y_{Df}))}}$$

$$y_{FP} \leq y_D \leq y_{Df} \tag{31a}$$

The second region IV solution is for the portion of region IV that is above the fracture, and is defined with a z-dependence.

$$P_{DIVz} = P_{Df} \frac{e^{-(b(z_D - z_{DF}))}}{e^{-(b(z_{FP} - z_{DF}))}}$$

$$z_{FP} \leq z_D \leq z_{Df} \tag{31b}$$

The reason that these particular expressions are used is that in order to solve the fracture equation and match the region boundaries the formation drawdown solutions are required in terms of either the fracture drawdown or the bounding region's functional form. When the angle goes to zero region IV decays to the fracture and there is then only x dependence for the flow in the fracture.

In equations (29) as the fracture angle goes to zero the parameter a goes to $\sqrt{s}$ and b goes to zero.

The partial differential equation describing the flow of fluid in the fracture plane is given by Equation (11) and (12). Using the partials of Equations (31) in Equation (11) and (12) gives the solution for the fracture flow in terms of the wellbore pressure, P_{Dw}

$$P_{Df\ x} = P_{Dw} \frac{e^{-(\gamma(x_{Df} - x_{FP}))}}{e^{-(\gamma(x_{Df} - r_D))}} \tag{32a}$$

$$P_{Df\ y} = P_{Dw} \frac{e^{-(a(y_{Df} - x_{FP}))}}{e^{-(a(y_{Df} - r_D))}} \tag{32b}$$

and

$$P_{Df\ z} = P_{Dw} \frac{e^{-(b(z_{FP} - z_{Dw}))}}{e^{-(bz_{Dw})}} \tag{32c}$$

where x_{FP}, y_{FP}, z_{FP} are the values of x_D, y_D, z_D in the fracture plane. From equations (29) and (13) we have for the fracture contribution to the Laplace transform of the wellbore dimensionless drawdown

$$P_{Dw} = \frac{\pi}{F_D s \gamma} \tag{33}$$

and γ is defined to be

$$\gamma^2 = \frac{1}{F_D}\beta + \frac{s}{\eta} \tag{34}$$

where

$$\beta = (1+tan(\theta))a+(1+cot(\theta))b \quad (35)$$

and a and b are given in equation (29).

Equation (34) dominates during the early time and through the bi-linear flow period. Then the formation linear flow begins to dominate. At that time the wellbore dimensionless drawdown is given by

$$p_{Dw} = \frac{\pi}{s(a+b)} \quad (36)$$

Equation (34) reduces to the finite conductivity result of Cinco et. al when $\theta = 0$ (vertical fracture), and equation (36) reduces to $\frac{\pi}{s^{3/2}}$, which has an inverse Laplace transform $P(t) = \sqrt{\pi t}$, i.e. the well-known 1/2 slope result for a vertical infinite conductivity fracture.

From inspection of the above equations we see that the flow to the fracture only has y dependence and the flow in the fracture only has x dependence for $\theta = 0$ (vertical fracture). These results hold true over all x, y, and z values and in the fracture.

Multiple Fractures

For multiple fractures we make the following assumptions:

a) the fractures are spaced by vertical amounts d1, d2, d3,···

b) the flow rates from the fractures are q1, q2, q3,···

c) the fractures have the fracture angles θ 1, θ 2, θ 3,···

d) the fractures are not intersecting

The solutions given above are for a single fracture centered on its coordinate system. Thus to superimpose the solutions from the i distinct fractures, the position of each fracture must be defined with respect to a grand coordinate system. For simplicity we choose the coordinate of the deepest fracture as the grand coordinate system, since all distances are then obtained from positive addition. This means that the fractures will be numbered from the deepest to the shallowest.

The distance from any point r to the coordinate system of the ith fracture will be

$$r-z_{fi} = \sqrt{(x-x_i)^2+(y-y_i)^2+(z-z_i)^2} \quad (37)$$

The total mass flowrate will be

$$q = \sum_{i=1}^{n} q_i \quad (38)$$

where n is the number of fractures.

The dimensionless pressure drawdown (buildup) at any point in space and time is given by the superposition of the pressure drawdowns (buildups) contributed by the flow to each fracture. The drawdown at the point r for the ith fracture is added for all n fractures to give

$$P_D(r,t) = \sum_{i=1}^{n} q_i P_{Di}(r-r_{fi},t) \quad (39)$$

P_D is the dimensionless drawdown obtained from the inverse Laplace transform of the solutions given in the previous sections of this report. The subscript on the ith fracture drawdown in the summation allows the fractures to have different angles (as long as they don't intersect).

COMPARISON OF MULFRAC RESULTS WITH PUBLISHED SPECIAL CASES

As the first step to check the equation, MULFRAC calculation results was compared with some published cases of single fracture model.

Erlougher's case (Vertical fracture model)

Figure 5 shows the comparison with Erlougher's fracture model (1977). This model is based on single infinite conductivity fracture. On the figure, Solid line shows MULFRAC calculation and circle plots shows Erlougher's result. The MULFRAC result shows good matching to the vertical model.

Cinco et al.'s case (Inclined fracture model)

Figure 6 shows the comparison with Cinco et al.'s fracture model (1975). This model is based on single inclined infinite conductivity fracture. On the figure, Solid line shows MULFRAC calculation and circle plots shows Cinco et al.'s result. The MULFRAC result shows good matching to the inclined fracture model.

CONCLUSIONS

In this report the solutions to the 3D problem of multiple high-angle fractures are given. The model solutions representing transient behavior of HAM fractures are defined in terms of 3D

rectilinear coordinates. The pressure behavior in the five regions approximates linear flow patterns and reduces the 3D problem to tractable equations. The five solution regions are linked at the region boundaries and provide a complete, unique solution in the Laplace domain.

The HAM fracture model equations include the finite conductivity of the fractures, and our solutions reduce to previously published results for the special case of vertical fractures and/or infinite-conductivity fractures. These new solutions do not give results for the limiting case of horizontal fractures, since further model development would be required for that case. The solutions are sufficiently general to allow the multiple fractures to have uneven spacing, different flow rates from each fracture, and different fracture angles. The elliptical intersection of the wellbore and the planar fracture is modeled by a rectangular source intersecting the fracture with length equal to the major axis of the ellipse. This assumption only results in approximation error if the fracture length is comparable to the wellbore radius.

A computer program, MULFRAC, has been provided to calculate the dimensionless drawdown at the wellbore. Solutions at any other point in space and for more than one fracture can easily be obtained by adding to the program the appropriate equations given in this report.

Since the MULFRAC program using this report was not extended to multiple fractures, we are starting to extend the program to multiple fractures model now.

NOMENCLATURE

The following symbols and definitions are used in the parameter definitions, below.

Variables

B formation volume factor

c fluid compressibility

F_D relative fracture conductivity $= \frac{k_f}{k}\frac{w}{x_f}$

h reservoir height

k matrix permeability

L fracture height measured in the plane of the fracture

P dimensionless Laplace transform of the pressure drawdown

q mass flow rate

r radius

s Laplace domain independent variable

t time

w fracture width

x x coordinate

y y coordinate

z z coordinate

θ angle of inclination from the z axis for inclined well

φ porosity

μ fluid viscosity

η_D diffusivity $= \frac{k}{\phi\mu c}$

Subscripts

D denotes dimensionless variable

f fracture variable or denotes fracture boundary

FP fracture plane

i initial value

w wellbore variable

WB wellbore surface in contact with the fracture

REFERENCES

Cinco, Ramey, and Miller (1975)." Unsteady-state Pressure Distribution Created by a Well with an Inclined Fracture"; SPE Paper 5591.

Cinco and Sameniego (1978). "Transient Pressure Analysis for Fractured Wells"; SPE Paper 7490.

Cinco, Sameniego, and Dominguez (1976). "Transient Pressure Behavior for a Well with a Finite-Conductivity Vertical Fracture"; SPE Paper 6014.

Erlougher (1977). "Advances in Well Test Analysis"; SPE Monograph, Volume 5.

Gringarten and Ramey (1974). "Unsteady State Pressure Distributions Created by a Well with a Single Horizontal Fracture, Partial Penetration, or Restricted Entry"; SPEJ; Vol. 14, No. 4, August 1974.

Gringarten, Ramey, and Raghavan (1974). "Unsteady-state Pressure Distributions Created by a Well with a Single Infinite Conductivity Vertical Fracture"; SPEJ; Vol. 14, No. 4, August 1974.

Strubhar, Fitch, and Glenn (1975). "Multiple Vertical Fractures from an Inclined Borehole", JPT May 1975.

Warren and Root (1963). "The Behavior of Naturally Fractured Reservoirs"; SPEJ September 1963.

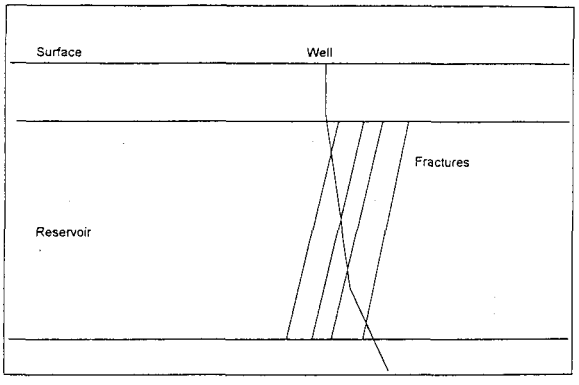

Figure 1. A generalized view of the HAM fractures.

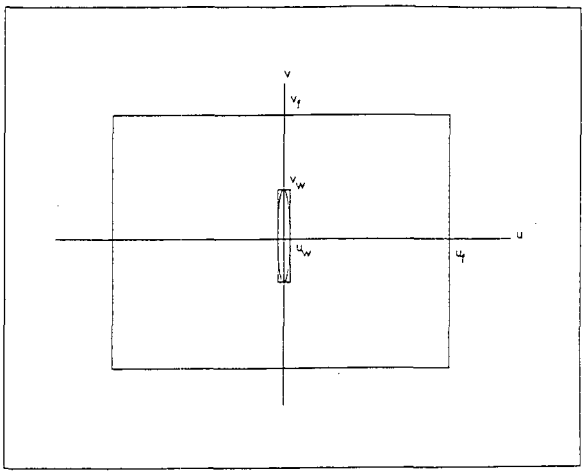

Figure 3. The fracture plane showing the elliptical wellbore-fracture intersection, the rectangular approximation to the ellipse, and the outline of the fracture rectangle.

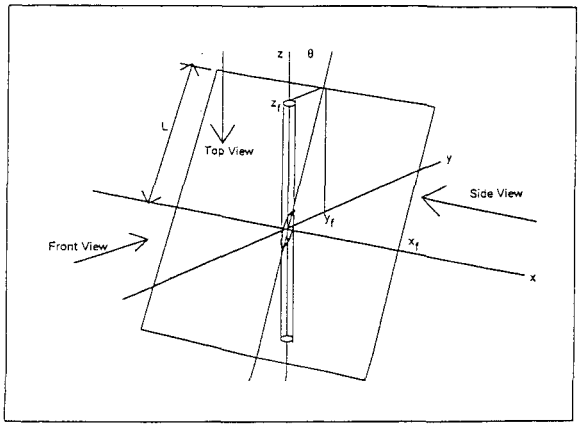

Figure 2. The inclined fracture geometry showing the fracture boundaries xf,yf,zf, and the elliptical intersection of the wellbore and fracture.

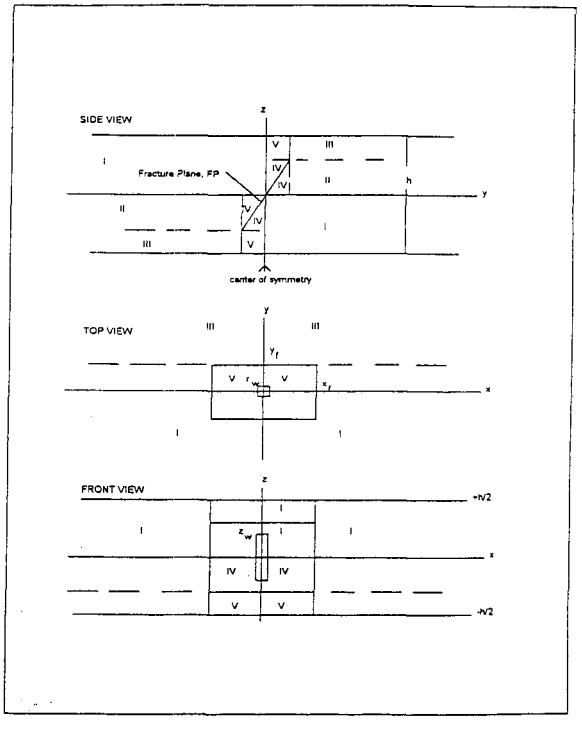

Figure 4. The geometry and boundaries defined for the inclined fracture, and the regions (I) through (V) that are defined for solution purposes.

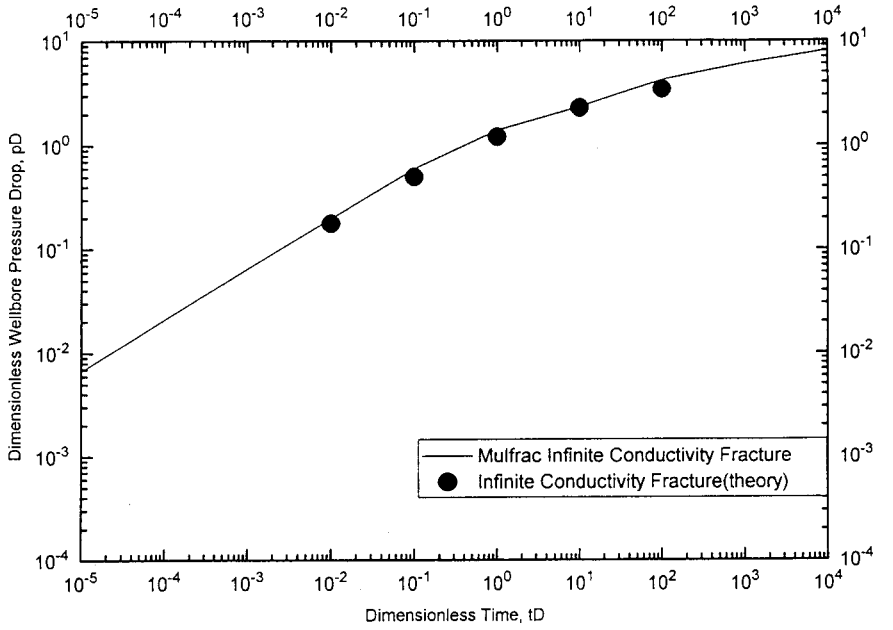

Figure 5. Infinite conductivity fracture comparison.

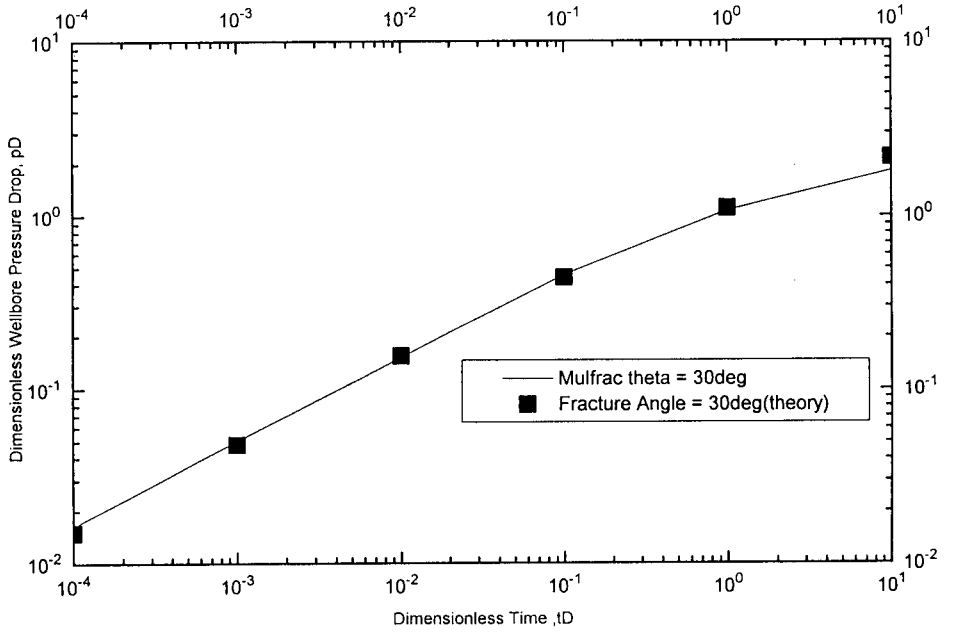

Figure 6. Angled fracture comparison.